Quantum charge transport in $Mo_6S_3I_6$ molecular wire circuits

M. Uplaznik, B. Bercic, M. Remskar, and D. Mihailovic
Jozef Stefan Institute, Jamova 39, SI-1000 Ljubljana, Slovenia
(Received 6 May 2009; revised manuscript received 8 July 2009; published 4 August 2009)

Charge transport measurements on flexible $Mo_6S_3I_6$ (MoSI) nanowires with different diameters in highly imperfect two-terminal circuits reveal systematic power-law behavior of the conductivity $\sigma(T,V)$ as a function of temperature and voltage. On the basis of measurements on a number of circuits we conclude that the behavior in *thin* wires can be most convincingly described by tunneling through Tomonaga-Luttinger liquid segments of MoSI wire, which is in some cases modified by environmental Coulomb blockade. The latter are proposed to arise from deformations or imperfections of the MoSI wires, which—in combination with their recognitive terminal sulfur-based connectivity properties—might be useful for creating subnanometer scale interconnects as well as nonlinear elements for molecular electronics.

DOI: 10.1103/PhysRevB.80.085402 PACS number(s): 73.23.−b, 73.22.−f

I. INTRODUCTION

While the transport properties of one-dimensional systems have been of great interest from the point of view of fundamental physics for some time,[1] recently, further interest in the transport properties of nanoscale one-dimensional systems was aroused because of their importance for the development of molecular electronics, where diverse molecular devices (switches, memory elements, sensors) all need to be self-assembled together with electrically conducting molecular scale wires. To be of practical use, the connectors need to have reliable contacts and also be able to withstand mechanical deformations while retaining their conducting properties. Until now there has been no recognized material which could be used for this purpose, and this has seriously impeded progress in the development of large scale molecular electronics in recent years.

In this paper we investigate the transport properties of $Mo_6S_3I_6$ molecular wires,[2] which have been recently shown to be very promising flexible molecular scale conductors. $Mo_6S_3I_6$ (MoSI) wires are air-stable one-dimensional inorganic cluster polymers (see Fig. 1), which are unique in that they enable covalent bonding to gold surfaces and organic molecules via sulfur atoms at the ends of each molecular wire.[4] Single molecular wires were also recently shown to self-assemble gold particles into critical scale-free networks.[5] Such molecular wires may expect their electron transport properties to be governed by quantum properties on the microscopic level. Thus, to make further progress in molecular electronics with MoSI connectors, we must first investigate and understand their molecular scale electronic transport properties. Earlier experimental work has shown metallic signatures, such as a low-frequency Drude response in the optical conductivity,[6] but relatively low room-temperature conductivities $\sigma \simeq 10$ S/m, which decrease with decreasing temperature.[7] Recently Venkataraman, Hong, and Kim[8] described electron transport measurements in multichannel $Li_2Mo_6Se_6$ nanowires with diameters in the range 7.2 to 12 nm in terms of a Tomonaga-Luttinger liquid (TLL) in contact with Fermi-liquid electrodes. In another related material $NbSe_3$, nanowires ranging between 30 and 300 nm in diameter have been observed to display similar power-law behavior, albeit over a rather limited range of temperature.[9] The extreme one-dimensional nature of the MoSI wires suggests that signatures of TLL behavior might also be observed in thick multistrand bundles and not only in very thin wires. On the other hand, we may expect that the electronic transport properties in MoSI wires might depart from ideal TLL behavior because of the deformable nature of the *S* bridges which link together the Mo_6 clusters into one-dimensional (1D) chains.[10]

In this paper we present a systematic study of MoSI wires of different diameter from 4 to 1000 nm, examining the *T* dependence, diameter dependence, and current-voltage characteristics at different temperatures. We are particularly in-

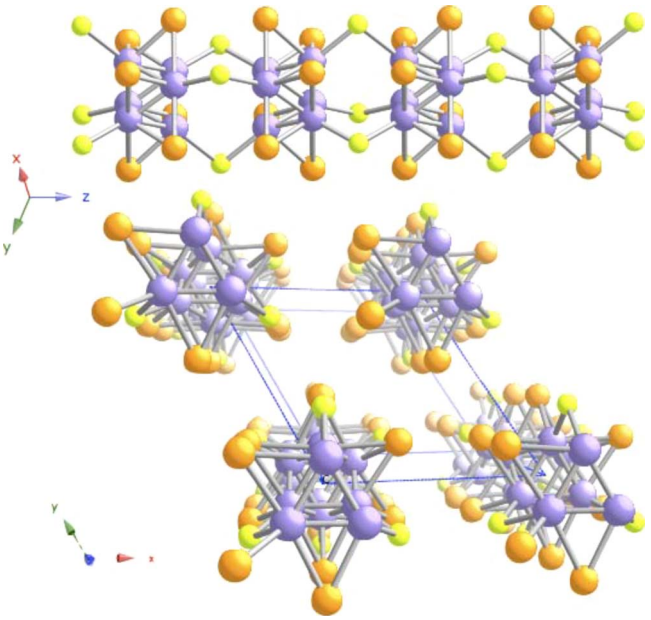

FIG. 1. (Color online) The Structure of $Mo_6S_3I_6$ wires. The axes are in the frame of the monoclinic space group $P\bar{1}$ (Ref. 3) with center-to-center distance of $d_0=0.958$ and the unit-cell length $c=1.197$ nm. The S atoms linking the Mo clusters form accordion-like deformable bridges and are shown by smaller yellow spheres, while the Mo clusters (violet spheres) are decorated on the outside by iodine (orange spheres).

terested in the behavior of realistic circuit configurations, with irregular wire geometries. The intrinsic flexibility of the MoSI wires, arising from their accordionlike structure[3,11] means that they bend easily to conform to surface contours. We have therefore focused on dielectrophoretically deposited thin wires over contacts in which the wires conform to the surface relief.

Considering the possible transport mechanisms, we confine ourselves to the common ones discussed in literature,[8,9] namely TLL tunneling,[1] environmental Coulomb blockade[12] (ECB), and variable range hopping (VRH) in the presence of Coulomb charging effects:[13]

(i) The T and V dependence for tunneling into a 1D TL liquid via Fermi-liquid metal contacts is given by

$$I = J_0 T^{1+\alpha} \sinh\left(\frac{\gamma eV}{2kT}\right)\left|\Gamma\left(1+\frac{\beta}{2}+i\frac{\gamma eV}{2\pi kT}\right)\right|^2 \quad (1)$$

where $\alpha=(g^{-1}-1)/4$, $\beta=(g+g^{-1}-2)/8$, J_0 is a constant, and the Luttinger parameter $g=v_F/v_\rho$. γ is a fitting parameter that accounts for the voltage drop over the circuit.[8,14] A collapsed diagram of the underlying transport characteristic is obtained by plotting $I/T^{\alpha+1}$ against eV/kT, where α is the slope of zero-voltage conductivity against temperature $\sigma=\sigma_0 T^\alpha$. β is the exponent for the high-voltage limit ($eV \gg kT$) arising from the power-law behavior $I \propto V^{\beta+1}$.

(ii) Unfortunately ECB models cannot be solved analytically for the general case, but the asymptotic behavior is very characteristic. The experimentally obtainable low-temperature behavior is given by

$$\sigma_{T\to 0,V\to 0} = \left(\frac{2}{g}+1\right)\frac{e^{-2\gamma/g}}{\gamma(2+2/g)}\frac{1}{R_T}\left[\frac{\pi}{g}\frac{e|V|}{E_C}\right]^{2/g}. \quad (2)$$

where E_C is the charging energy, $g=G_0/G$, G is the frequency-independent conductance, $G_0=2e^2/h$ and R_T is the tunneling resistance.[12] For low voltages and temperatures the current follows a power-law behavior $I \propto V^{2/g}$. For high voltages (but low temperatures),

$$I(V) = \frac{1}{R_T}\left[V - \frac{e}{2C} + \frac{g}{\pi^2}\frac{e^2}{4C^2}\frac{1}{V}\right] \quad (3)$$

which gives a linear $I-V$ dependence at high V, so the derivative dI/dV is expected to approach an asymptotic constant value of $1/R_T$.[7,12] It also gives a nonzero intercept for $I=0$ given by the charging energy $e^2/2C$.

(iii) For the variable range hopping mode, a plot of $\ln(G)$ (for low voltage) against $T^{-\lambda}$ yields curves which become linear with the correct hopping exponent λ. The fits to the data typically give a large error in the exponents, so to extract the best value of λ, fits to the data are tested statistically by calculating Pearson's correlation coefficients.

Rather than choosing a few measurements which obey one or another type of behavior, we present here a summary of a number of experiments, to try and understand the different types of behavior that can arise in nanoscale circuits with MoSI wires.

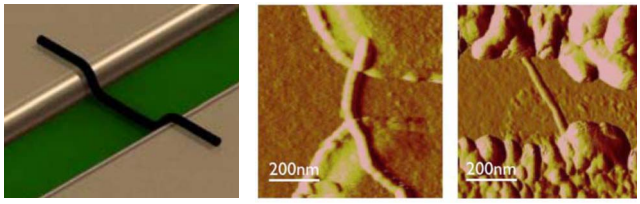

FIG. 2. (Color online) A schematic diagram of the circuit geometry (left). AFM topographic images of the thin wires after annealing. The wire diameters (from the height profile) are 4.2 and 4 nm for samples na23 (middle) and na27 (right), respectively. The roughness of the Ni electrodes appears after annealing and is caused by metal aggregation during the high-temperature annealing process.

II. EXPERIMENTAL DETAILS

The thin wires were prepared according to the method reported by Nicolosi *et al.*[15] by repeated dispersion and dilution. The dispersion procedure separates the wires into two distinct categories: thin wires with diameters $4<D<10$ nm and thick multichannel bundles with $100<D<1000$ nm.[15] In the ultrasonic bath processing procedure, the defective wires break up into shorter segments, leaving less defective long thin wires in solution. The individual strands within the thin wires may thus be expected to have significantly fewer imperfections than within the thick bundles, which may result in different electron transport behavior in thick and thin wires. This should be evident in the room-temperature conductivity ($\sigma_{300\ \mathrm{K}}$) as well as the T dependence and $I-V$ systematics.

The wires were dielectrically deposited typically over nickel electrodes prepared by electron beam lithography by placing a drop of solution over the electrodes and applying a 50 Hz ac electric field to the electrodes. The entire circuits were then annealed in vacuum at 700 C for an hour. The circuits after annealing are shown in Fig. 2. Typical resistances of the nanowires at room temperature were between 100 kΩ and 100 MΩ. Care was taken to ensure good thermal contact of the sample with the cryostat cold finger.

III. EXPERIMENTAL RESULTS AND ANALYSIS

A. Thin wires

Two thin wire circuits labeled na27 and na23 (shown in Fig. 2) illustrate the most common type of behavior observed in a number of measured circuits with diameters ranging from $d\sim 4$ to 15 nm. The room-temperature conductivity $\sigma_{300\ \mathrm{K}}$ for na27 and na23 was 3710 and 11900 S/m, respectively. Their $I-V$ characteristics at temperatures between 18 and 300 K are shown in Figs. 3(a) and 4(a) and exhibit qualitatively different behavior. In the case of sample na27, the $I-V$ curves show characteristic inverted S shaped curves whose curvature is strongly T dependent. In contrast, circuit na23 shows a clear J-like shape characteristic. (Other circuits we have measured show behavior in between these two extremes).[16] The T dependence of the conductance $G=dI/dV$ at $V=0$ is shown in Figs. 3(b) and 4(b). The line is a fit to a power law $G=G_0T^\alpha$ where $\alpha=2.3$ and 3.5, respec-

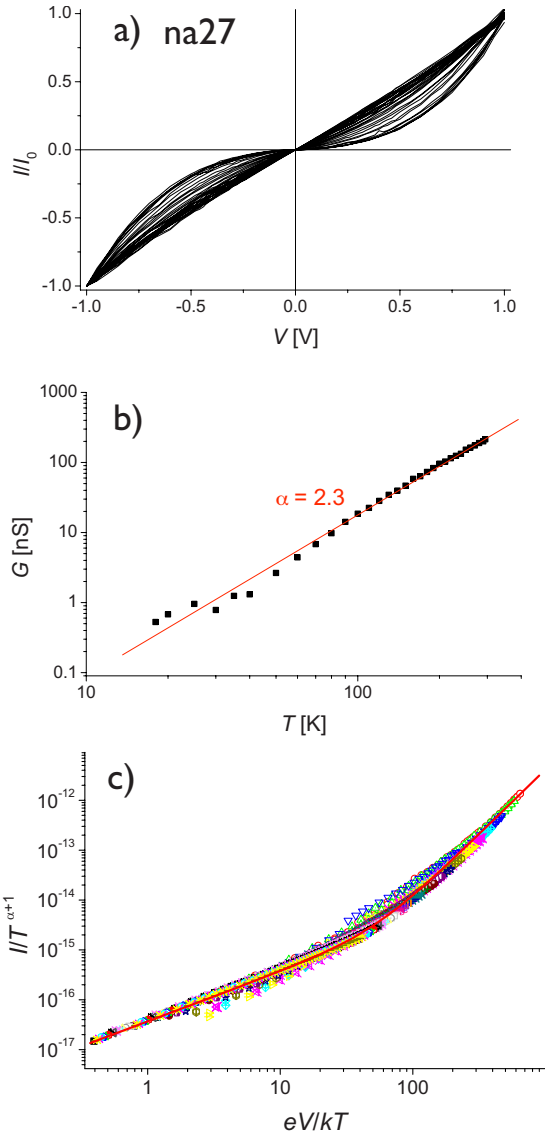

FIG. 3. (Color online) (a) Normalized $I-V$ characteristics of sample circuit labeled na27 (d=4 nm) at different temperatures. (The current was arbitrarily normalized at 1 V for all curves. At 295 K, I_0=230 nA.) (b) The zero-bias conductance (slope of $I-V$ curve at low bias, $V=\pm 20$ mV) as a function of temperature on a log-log plot. (c) A plot of $I/T^{\alpha+1}$ vs eV/kT shows the data collapse onto a single curve. Here $J_0=7.7\times10^{-16}$ A, α=2.3, β=1.6, and γ=1/18.

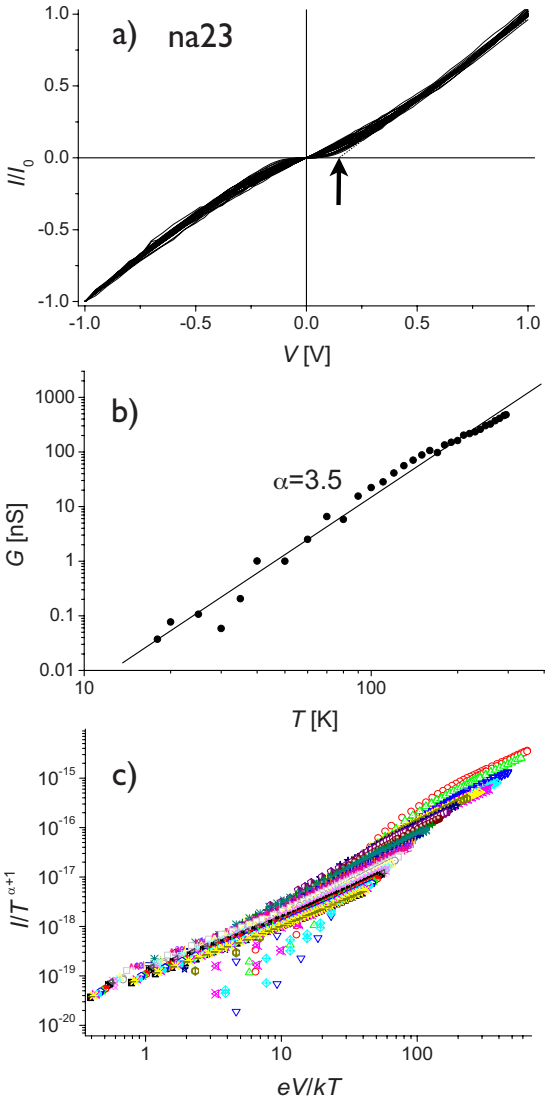

FIG. 4. (Color online) (a) Normalized $I-V$ characteristics of sample circuit labeled na23 (d=4.2 nm) at different temperatures. (The current was arbitrarily normalized at 1 V for all curves. At 295 K, I_0=620 nA.) The arrow shows the extrapolated voltage corresponding to $V=e/2C$. (b) A log-log plot of the zero-bias conductance measured in the range $V=\pm 20$ mV as a function of temperature. (c) A plot of $I/T^{\alpha+1}$ vs eV/kT do *not* show the data collapse exhibited by circuit na27 in Fig. 3(c) for any set of parameters in Eq. (1).

tively. The data follow the power-law fit reasonably well, but do not give a perfect fit over the entire range of T. Plotting the entire data set $I/T^{\alpha+1}$ against eV/kT according to the TLL prediction, for na27 we see that the data collapse quite well onto a single curve [Fig. 3(c)], where β=1.6 in Eq. (1) are obtained from the fit. The behavior of na23 is very different to na27. It gives no such TLL collapse [Fig. 4(c)], indicating clear departure from TLL predictions. (Overall, approximately half our circuits showed the TLL collapse.)

Attempting to fit the ECB model to the data, we would expect the I/V slope to cross over from $\sim 2/g$ at low voltages to $1/R_T$ at high voltages. Correspondingly, the derivative dI/dV should show a systematic T-independent crossover from $2/g-1$ to 0 corresponding to the low- and high-voltage limits, respectively. We plot dI/dV vs V, in Figs. 5(a) and 5(b), respectively, for na23 and na27. Circuit na27 shows a rather small variation of dI/dV with V over the entire range of V and T (note the small values on the log scale on the dI/dV axis), quite unlike the ECB model predictions. In contrast, na23 shows a systematic variation with V, which for low temperatures is not far from what is expected on the basis of ECB theory: at low V, $dI/dV\sim 0$ (within experimental error), but clearly saturating at high V.

For completeness, attempting to fit the data to the VRH model, we first plotted $\ln(G)$ (for low voltage) against $T^{-\lambda}$ for different $\lambda=1/4$ to 1, according to the VRH model (Fig. 6). Making a statistical evaluation using Pearson's correla-

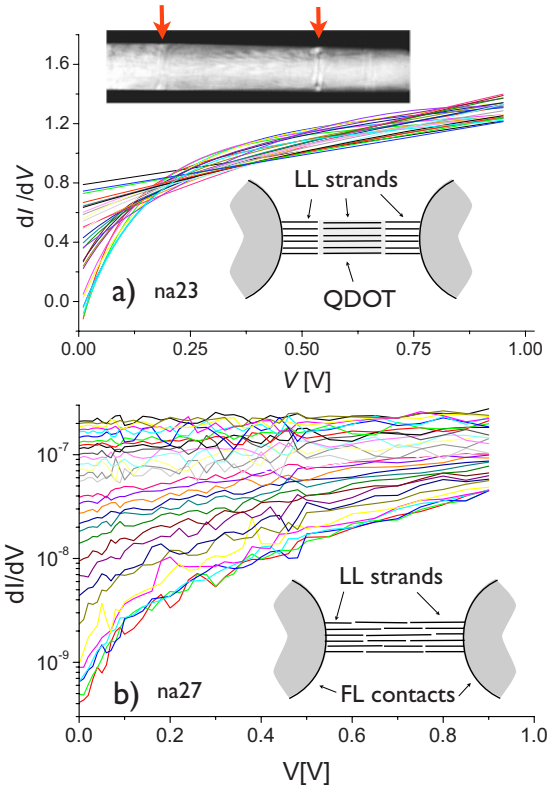

FIG. 5. (Color online) The derivatives dI/dV obtained from the normalized $I-V$ data plotted in Figs. 3(a) and 4(a) for circuits (a) na23 and (b) na27 at different temperatures. The derivative at low V increases in both cases, as T increases from 18 to 300 K. The insert in (a) shows a high-resolution transmission electron microscope image of a single pristine wire (as-synthesized) with a diameter of 124 nm. The defects in the structure are clearly visible as streaks across the wire which may cause the formation of a QDOT (see discussion).

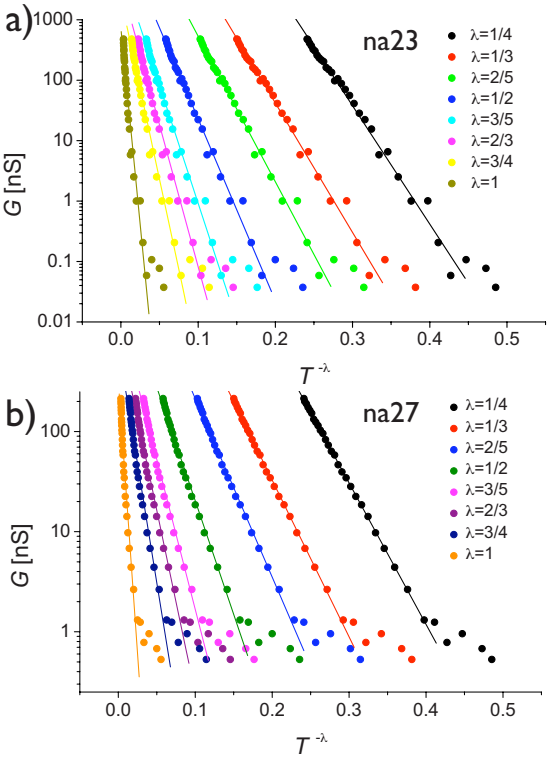

FIG. 6. (Color online) T dependence of the conductance G plotted as a function of $T^{-\lambda}$ with different exponent λ for sample circuits (a) na23 and (b) na27.

tion test, we find that the best fit is with $\lambda=1/4$ for na27 and $\lambda=1/3$ for na23. Such small values of λ within VRH models would imply the dominance of three-dimensional hopping processes, which is clearly inconsistent with the nature of the system investigated here. The calculation of Fogler *et al.*[13] considered a quasi-1D wire with a finite density of impurities modeled by a series of weakly coupled quantum dots. They predict power-law behavior of the current for both T and V, as $I \propto V^{\beta+1}$ at high V and $I \propto T^{\alpha}V$ at low V with $\alpha \gg \beta \gg 1$. The model holds for a large number of parallel statistically independent conduction channels, where power laws are not obscured by the fluctuations of G. This case is fulfilled here for thick wires, with bundle diameters between 100 nm and 1 μm might have 10^4 to 10^6 conducting channels. However, the prediction that $\beta \gg 1$ is not fulfilled here for either the thin or the thick multichannel bundles discussed in the next section, suggesting that this model may not be applicable for describing MoSI circuits.

B. Thick bundles

Ubiquitous feature of the thick wire bundles ($d=100 \sim 1000$ nm) is their linear $I-V$ characteristic from 18 to 300 K.[7] The room-temperature conductivity σ_0 is typically three orders of magnitude *smaller* than for the thin wires, around 1–10 S/m. This is taken as a clear indication that only a small fraction f of the molecular strands in the bundle contribute to the transport. Confirming earlier preliminary measurements, the T dependence was not very well described by a 1D VRH model.[7] The new systematic data on many circuits now confirms this. The dependence of the conductivity is shown in Fig. 7 for a number of bundles of different diameter. Surprisingly, the data for the different bundles all appear to follow power-law behavior $\sigma=\sigma_0 T^{\alpha}$ quite well. Moreover, a systematic trend is observed, whereby the larger diameters have a smaller exponent α, an indication that the numbers of conducting channels scales with diameter[1] (Fig. 8).

IV. DISCUSSION

In circuit na27 the TLL prediction can be confirmed with some degree of confidence by the collapsed plot of $I/T^{\alpha+1}$ vs eV/kT. For tunneling from a Fermi liquid into a perfect TLL without defects, the model prediction is that $\alpha=\beta$. Imperfections, such as deformations and kinks or stoichiometric defects break up the wire into TLL segments, which introduces TLL-TLL tunneling between these segments,[8] for which the predicted ratio changes to $\alpha=2\beta$. The measured value for na27 is $\alpha/\beta=1.45\pm0.1$. A similar circuit with a wire diameter of 5 nm (na12, not shown) gives a near-identical collapse as na27 with $\alpha/\beta=2.00\pm0.1$.

The exponent α for a N-channel wire is given by TLL theory[17] as:

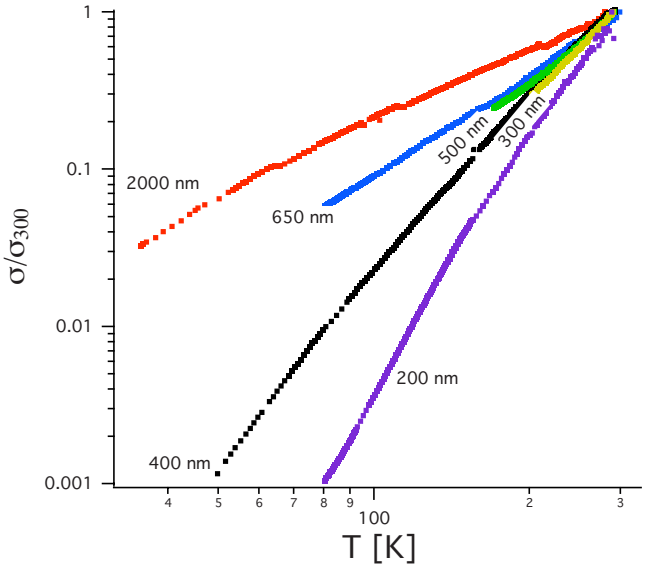

FIG. 7. (Color online) The normalized conductance G/G_0 of a large number of thick wires, with $d=200\sim2000$ nm. In two measurements, a break is observed, which is believed to be strain-induced change in the number of conducting channels.

$$\alpha = \frac{2}{N}\left[\sqrt{1+\frac{2N}{g^2}}-1\right], \tag{4}$$

where g is the electron-electron interaction parameter. The number of conducting channels N in a nanowire of diameter d can be written as $N=2f\frac{D^2}{a^2}$, where a is the lattice constant and f is the fraction of molecular wires which actually carry current without interruption. For circuit na27, using $f=1$, $\alpha=2.3$, and $N=16$ channels (for $d=4$ nm), we calculate $g=0.21$. This is slightly larger than the value 0.15 obtained by Venkataraman *et al.* for $Li_2Mo_6Se_6$ nanowires. Other wires which we have measured have α between 2 and 3.5, giving a range of $0.09<g<0.27$. Comparing this with g estimated from materials parameters, we can use the expression from the Coulomb charge screening model[17] $g^2=v_F R_0 C_0$, where $v_F=7\times10^5$ m/s is the Fermi velocity calculated by density functional theory (DFT) calculations, R_0 is the resistance quantum and the single wire capacitance per unit length is $C_0=\frac{2\pi\epsilon_r\epsilon_0}{\ln[4t/d_0]}$. Using $\epsilon_r=3.9$ for the Si oxide layer of thickness $t=600$ nm, we obtain $g=0.49$. In this estimate, the DFT value of v_F is likely to be overestimated, which may account for a large part of the discrepancy between the values obtained directly from the measurements. It has also been noted previously that the static Coulomb screening model overestimates g.[8]

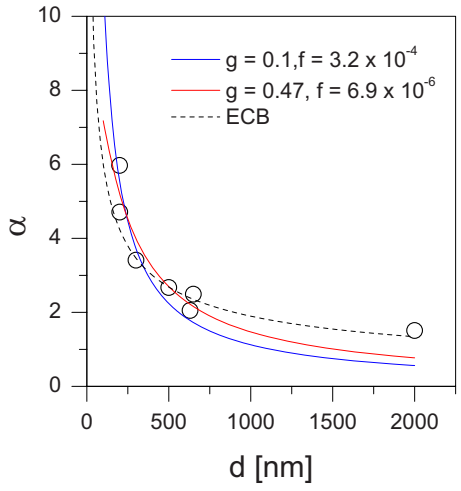

FIG. 8. (Color online) The dependence of the temperature exponent α of thick wires on bundle diameter d from the data in Fig. 7.

The data in Fig. 8 for the thick wires can be fit using the expression Eq. (4). A range of values of g can be obtained from the fits to the present data, $0.1<g<0.5$ with corresponding filling factors $10^{-5}<f<10^{-4}$. Values outside this range of g cannot be made to fit the data. However, since the $I-V$ characteristics are ubiquitously linear, for the thick wires, this in itself cannot be taken as proof for TLL behavior.

The low value of σ_0 in thick wires is assumed to be related to imperfections on the wires. It suggests that the transport along the wires is dominated by tunneling between TLL segments. In fact the resistance of both thick and thin wires is typically of the same order of magnitude, which suggests that in the thick bundles only a very small number of wires are uninterrupted, or that only strands on the outside of the bundle are conducting, with the inner strands being unreachable due to the extremely small perpendicular intermolecular hopping rates within each wire.

Turning to the case of na23, which shows clear characteristics of ECB behavior, the intercept of the $I-V$ curve at $I=0$ gives $V=\frac{e}{2C}\simeq0.15$ V and consequently $C\simeq5.3\times10^{-19}$ F. Comparing this quantum dot (QDOT) capacitance with an estimate of C for a single wire over a Si ground plane with a 600 nm SiO_2 insulating layer and length $L=265$ nm between contacts, we have $C\simeq8\times10^{-18}$, for na23. Depending on what we assume for the QDOT shape, its size appears to be some fraction $(\sim1/10)$ of the distance between the electrodes.

Considering the possible origin of the ECB behavior and the observed departures from the predicted TLL characteristics, we can imagine imperfections and breaks of continuity in the wires of diverse origin. The most obvious and unavoidable effect arises from the deformation of the nanowires adapting to the relief of the contacts (Fig. 2). Their inherent flexibility allows for a substantial deformation, which is accompanied by significant changes in electronic structure near the Fermi energy.[10,18] We can thus envisage that the deformations can lead to breaks in the continuity of individual channels, and as a result the formation of a QDOT in between the breaks. In this case the ECB capacitance would scale with the distance between electrodes. Another effect, which might be important, arises from the intrinsic tendency of the wires to form discontinuities in the structure, as shown in the high-resolution transmission electron microscopy (HRTEM) image in Fig. 5(a). Clear stripes are sometimes observed across the wire bundles, which arise from stacking faults which appear during the growth process.

Indeed such compositional ordering has been recently theoretically predicted.[19] HRTEM diffraction analysis shows that the structure of the wire is identical on both sides of the fault, but clearly continuity is broken at these points. Sections in between the faults may thus act as QDOTs, leading to the ECB behavior we observe. Considering that the distance between faults may be a few tens of nanometers, the comparison of QDOT capacitance with the static capacitance calculated in the previous paragraph suggests this effect may also be important.

V. CONCLUSION

One of our objectives has been to determine how imperfect, bent, and deformed MoSI wires might behave in molecular scale circuits such as may form upon self-assembly.[5] It is clear from the present experiments that quantum transport dominates their behavior. The TLL model with its characteristic data collapse of the $I-V$ characteristics at different temperatures appears to hold well for a significant proportion of the thin wire circuits. At the same time clear signatures of the ECB predicted J-shaped $I-V$ curves are also occasionally observed. Discontinuities in the wires either as a result of bending, and/or structural stacking faults within the wire are believed to cause the formation of QDOTs, which lead to the occasional occurrence of ECB behavior. The diameter of the present MoSI wire bundles is small enough to allow covalent S bonding to individual molecules,[4] so for the construction of molecular scale circuits, where thin and relatively short wires are of interest, they may potentially revolutionize molecular electronics. A point of interest is the possibility of making variable sizes of QDOTs with MoSI wires by stretching them over appropriately sized regular topological features to produce arrays of QDOTs. The other possibility of creating single QDOTs by using the tip of an atomic force microscope, was already recently demonstrated.[20]

ACKNOWLEDGMENTS

We wish to thank D. Vengust for providing samples of MoSI nanowires and J. Strle for proofreading the manuscript.

[1] J. Voit, Rep. Prog. Phys. **58**, 977 (1995) and references within.
[2] D. Vrbanić *et al.*, Nanotechnology **15**, 635 (2004); for a review, see: D. Mihailovic, Rep. Mater. Sci. **54**, 309 (2009).
[3] V. Nicolosi *et al.*, Adv. Mater. **19**, 543 (2007).
[4] I. M. Ploscaru, S. Jenko Kokalj, M. Uplaznik, D. Vengust, D. Turk, A. Mrzel, and D. Mihailovic, Nano Lett. **7**, 1445 (2007).
[5] J. Strle, D. Vengust, and D. Mihailovic, Nano Lett. **9**, 1091 (2009).
[6] D. Vengust, F. Pfuner, L. Degiorgi, I. Vilfan, V. Nicolosi, J. N. Coleman, and D. Mihailovic, Phys. Rev. B **76**, 075106 (2007).
[7] M. Uplaznik, B. Bercic, J. Strle, M. I. Ploscaru, D. Dvorsek, P. Kusar, M. Devetak, D. Vengust, B. Podobnik, D. Mihailovic, Nanotechnology, **17**, 5142 (2006); B. Berčič *et al.*, Appl. Phys. Lett. **88**, 173103 (2006).
[8] L. Venkataraman, Yeon Suk Hong, and P. Kim, Phys. Rev. Lett. **96**, 076601 (2006).
[9] E. Slot, M. A. Holst, H. S. J. van der Zant, and S. V. Zaitsev-Zotov, Phys. Rev. Lett. **93**, 176602 (2004).
[10] I. Vilfan and D. Mihailovic, Phys. Rev. B **74**, 235411 (2006).
[11] T. Meden *et al.*, Nanotechnology **16**, 1578 (2005).
[12] M. H. Devoret and H. Grabert, in *Single Charge Tunneling*, edited by H. Grabert and M. H. Devoret, NATO Advanced Studies Institute, Series B: Physics (Plenum, New York, 1992), Vol. 294.
[13] M. M. Fogler, S. Teber, and B. I. Shklovskii, Phys. Rev. B **69**, 035413 (2004).
[14] M. C. Bockrath, D. H. Cobden, J. Lu, A. G. Rinzler, R. E. Smalley, L. Balents, and P. L. McEuen, Nature **397**, 598 (1999).
[15] V. Nicolosi, D. Vrbanic, A. Mrzel, J. McCauley, S. O'Flaherty, C. McGuinness, G. Compagnini, D. Mihailovic, W. J. Blau, and J. N. Coleman, J. Phys. Chem. B **109**, 7124 (2005).
[16] M. Uplaznik, Ph.D. thesis, Univ. of Ljubljana (2009).
[17] K. A. Matveev and L. I. Glazman, Phys. Rev. Lett. **70**, 990 (1993).
[18] I. Popov, T. Yang, S. Berber, G. Seifert, and D. Tomanek, Phys. Rev. Lett. **99**, 085503 (2007).
[19] T. Yang, S. Berber, and D. Tomanek, Phys. Rev. B **77**, 165426 (2008).
[20] A. Hassanien, M. Tokumoto, A. Mrzel, D. Mihailovic, and H. Kataura, Physica E **29**, 684 (2005); H. W. Ch. Postma, T. Teepen, Zhen Yao, M. Grifoni, and C. Deeker, Science **293**, 76 (2001).